
Coherent and Multi-modality Image Inpainting via Latent Space Optimization

Lingzhi Pan¹, Tong Zhang^{2*}, Bingyuan Chen¹, Qi Zhou¹, Wei Ke¹, Sabine Süsstrunk²,
Mathieu Salzmann²

¹ Xi'an Jiaotong University ² EPFL

<https://pilot-page.github.io>

Abstract

With the advancements in denoising diffusion probabilistic models (DDPMs), image inpainting has significantly evolved from merely filling information based on nearby regions to generating content conditioned on various prompts such as text, exemplar images, and sketches. However, existing methods, such as model fine-tuning and simple concatenation of latent vectors, often result in generation failures due to overfitting and inconsistency between the inpainted region and the background. In this paper, we argue that the current large diffusion models are sufficiently powerful to generate realistic images without further tuning. Hence, we introduce PILOT (inPainting vIa Latent OpTimization), an optimization approach grounded on a novel *semantic centralization* and *background preservation loss*. Our method searches latent spaces capable of generating inpainted regions that exhibit high fidelity to user-provided prompts while maintaining coherence with the background. Furthermore, we propose a strategy to balance optimization expense and image quality, significantly enhancing generation efficiency. Our method seamlessly integrates with any pre-trained model, including ControlNet and DreamBooth, making it suitable for deployment in multi-modal editing tools. Our qualitative and quantitative evaluations demonstrate that PILOT outperforms existing approaches by generating more coherent, diverse, and faithful inpainted regions in response to provided prompts.

1 Introduction

The development of text-to-image models like Stable Diffusion [24] and DALL-E 2 [23] has led to remarkable visual results, paving the way for editing images through text inputs [5]. However, text-based editing alone often falls short of achieving the precise modifications desired by users. Consequently, multimodal control tools such as ControlNet [40] and IP-Adapter [38] address this limitation by enabling more diverse and accurate image generation controls. Despite these advancements, these methods are unable to insert arbitrary edits that seamlessly fit into the image, making diffusion model-based inpainting essential for preserving the background while altering specific regions.

Utilizing diffusion models for inpainting is primarily achieved via two main approaches: model fine-tuning and latent/pixels blending. Fine-tuning methods either further tune the diffusion model [24, 34, 32] or train additional neural networks as conditions for the diffusion model [39] according to the loss from unmasked/background region. They often produce outputs misaligned with the original domain or require retraining for unseen conditions, limiting their practicality and effectiveness. In contrast, latent blended diffusion methods [1] simply concatenate the latent vectors of the unmasked region and masked region with conditions guided. Although efficient and compatible with multiple conditions,

*Corresponding author

this simple mixing strategy usually leads to semantic inconsistency because it does not fully account for the complex relationships and dependencies between different image regions. Therefore, we aim to combine the advantages of both approaches, achieving efficiency and high-quality image generation. Considering the potent generative and expressive capabilities of current diffusion models, we believe that finding latent vectors that can create coherent inpainted images while adhering to prompts across various modalities is a more effective solution.

To achieve this objective, we introduce a novel latent space optimization framework named PILOT. Unlike simple blending techniques [2, 1], PILOT starts with classifier-free diffusion and optimizes both the conditional and unconditional latent vectors on the fly during the generative process by correcting the gradients with our novel cost functions: background preservation loss and semantic centralization loss. During the optimization, we leverage one-step reconstruction ($x_t \rightarrow x_0$) to construct the losses. The background preservation loss ensures that the background generated by the unconditional vectors remains consistent with the original, while the semantic centralization loss makes the conditional vectors closely align with the prompt in the inpainted region while maintaining similarity to the unconditional ones. This interaction between the two vectors ensures coherent, high-quality image generation that meets user specifications across various scenarios. Furthermore, we observe that the early stage of the generative process captures semantic information, while the later stages focus on adding finer or high-frequency details [41, 42]. Hence, we introduce a coherence scale parameter γ to balance efficiency and generation quality. This allows us to generate a high-quality inpainted image with multiple prompts from different modalities within 10 seconds on a single GPU. Notably, due to the optimization nature of our method, PILOT enables personalized text-to-image models trained by DreamBooth [25] or LoRA [12] to perform subject-driven inpainting.

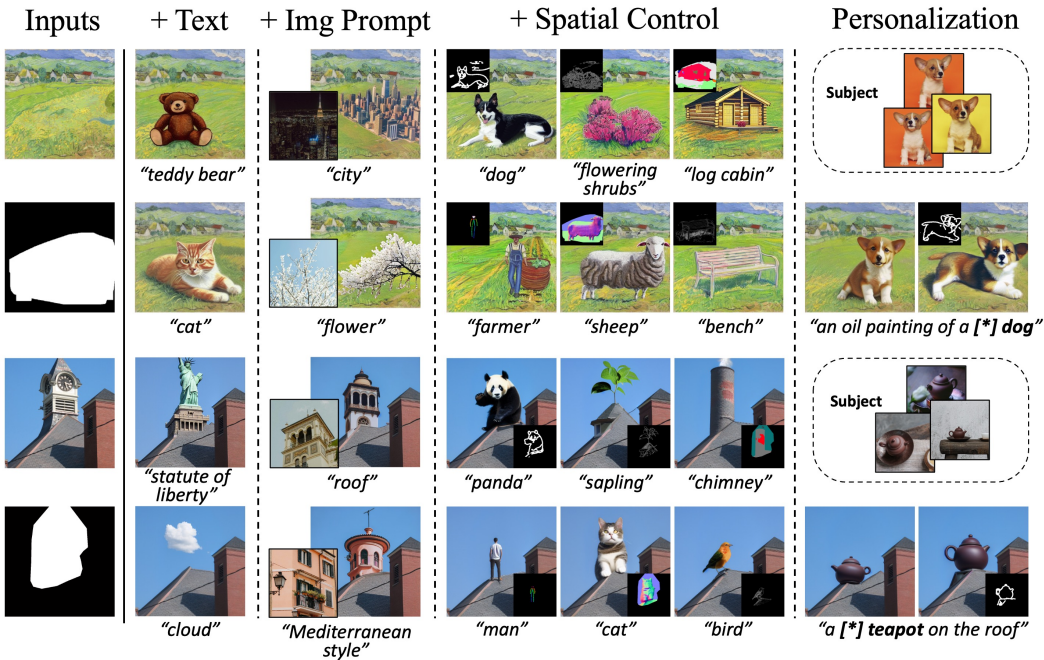


Figure 1: We showcase the versatility of our approach with single and multiple modalities by generating images in various settings, such as text, text + image prompt, text + scribbles, and subject as reference.

In summary, our contributions can be outlined as follows:

- We introduce an efficient inpainting framework, PILOT, which optimizes latent vectors during the reverse process to generate high-quality and coherent edits on images.
- We design novel losses to achieve high fidelity to user-provided prompts while maintaining coherence between the inpainting area and the background region.
- To balance generation speed and image quality, we propose a mixed reverse diffusion pipeline, utilizing a parameter γ to control the number of optimization steps and blending.

Our extensive experimental results demonstrate that our method outperforms the SOTA inpainting techniques, leading to high coherence and diversity.

2 Related Work

Text-guided Image Editing. Recently, many deep learning methods based on text-to-image diffusion models have been employed for image editing tasks [26, 3, 20]. Inversion-based methods [17, 33, 14, 29, 30] transform the source image into a noisy latent vector through the reverse sampling process of diffusion and utilize the noisy latent vector as a starting point for denoising and incorporating additional controls during the generation process. Other methods such as Prompt-to-Prompt [8] modify the cross-attention layer using the information from the source image. To create a more user-friendly interactive image editing model, InstructPix2Pix [5] trains a conditional diffusion model to follow human-written instructions for image editing during the forward pass. However, these methods heavily depend on the correspondence between text and regions, often resulting in undesired changes in arbitrary areas. This limitation restricts their effectiveness for local editing.

Multi-modality Image Generation. To achieve more controllable generation, many methods have trained one or more plug-and-play adapters to incorporate control information beyond text [40, 43, 18, 38, 31]. These adapters encode information from other modalities along with the denoising latent and integrate it into the intermediate and output layers of the original network, thereby guiding the generation process. ControlNet [40] and T2I-Adapter [18] add spatial controls such as human sketch to the generation process of Stable Diffusion. IP-Adapter [38] introduces adapted modules with decoupled cross-attention to embed the content and style of given images into the model. These methods can generate high-quality images with good controllability. However, for local image generation tasks, they often rely on latent blending [1] techniques. Although they achieve controlled generation, the visual coherence between the generated local region and the surrounding areas is often lacking.

Text-guided Image Inpainting. In the realm of image editing, methods originally developed for image inpainting are often repurposed to enable the editing of specific local regions within an image. By delineating a mask region, users can direct the generation of desired effects within that area using textual prompts. Some methods leverage image-to-image models trained with the original image and mask as input conditions, such as GLIDE [19] and Imagen Editor [32]. Uni-paint [37] further allows different modalities as inputs to guide the inpainting generation. These approaches fine-tune text-guided diffusion models to facilitate the inpainting of regions in images conditioned on text. However, in practice, fine-tuning methods pose challenges such as difficulty in tuning, susceptibility to overfitting, and the generation of unrealistic images. Moreover, fine-tuning large-scale models can be computationally expensive.

Additionally, numerous methods focus on blending information from known regions into noisy latent representations. Blended Diffusion [2] imposes additional constraints on the noisy latent vector, blending noisy versions of the source image with the generated noisy latent vector throughout the denoising process. Blended Latent Diffusion [1] allows the Latent Diffusion Model to perform local image edits by conducting blending in the latent space. PFB-Diff [13] employs multi-level feature blending and introduces an attention masking mechanism in the cross-attention layers to confine the region affected by specific words. However, despite their efficiency and extensibility, these methods often produce unsatisfactory results, leading to incoherent images.

In contrast, PILOT optimizes the latent space to achieve efficiency while generating high-quality results. Importantly, our approach can optimize latent vectors within any pre-trained latent diffusion model using arbitrary adapters, enabling multi-modality and precise controllability.

3 Preliminaries

In the theory of diffusion models [10], the forward Markovian noising process is defined to introduce noise to the initial input image, denoted by x_0 , across multiple time steps t . This is expressed as

$$q(\mathbf{x}_t|\mathbf{x}_{t-1}) = \mathcal{N}(\mathbf{x}_t; \sqrt{\alpha_t}\mathbf{x}_{t-1}, (1 - \alpha_t)\mathbf{I}), \quad (1)$$

$$q(\mathbf{x}_{1:T}|\mathbf{x}_0) = \prod_{t=1}^T q(\mathbf{x}_t|\mathbf{x}_{t-1}), \quad (2)$$

where α_t represents the variance that regulates the noise schedule, and T denotes the total number of steps. For a sufficiently large value of T , \mathbf{x}_T will converge towards standard Gaussian noise.

Given the independence of transitions in a Markov process, \mathbf{x}_t can be obtained directly by adding noise to \mathbf{x}_0 as

$$q(\mathbf{x}_t|\mathbf{x}_0) = \mathcal{N}(\mathbf{x}_t; \sqrt{\bar{\alpha}_t}\mathbf{x}_0, (1 - \bar{\alpha}_t)\mathbf{I}), \quad (3)$$

$$\mathbf{x}_t = \sqrt{\bar{\alpha}_t}\mathbf{x}_0 + \sqrt{1 - \bar{\alpha}_t}\boldsymbol{\epsilon}_t, \quad (4)$$

where $\bar{\alpha}_t = \prod_{i=1}^t \alpha_i$. The conditional probability distribution was derived by Ho *et al.* [10] to reverse the process and given by

$$p_\theta(\mathbf{x}_{t-1}|\mathbf{x}_t) = \mathcal{N}(\boldsymbol{\mu}_\theta(\mathbf{x}_t, t), \boldsymbol{\Sigma}_\theta(\mathbf{x}_t, t)), \quad (5)$$

$$\boldsymbol{\mu}_\theta(\mathbf{x}_t, t) = \frac{1}{\sqrt{\alpha_t}}\left(\mathbf{x}_t - \frac{\beta_t}{1 - \bar{\alpha}_t}\boldsymbol{\epsilon}_t\right), \quad (6)$$

where $\beta_t = 1 - \alpha_t$. To approximate the noise, a deep neural network $\boldsymbol{\epsilon}_\theta(\mathbf{x}_t, t)$ is trained to predict $\boldsymbol{\epsilon}_t$ for a random noise level of \mathbf{x}_t using the loss function

$$\mathcal{L} = \mathbb{E}_{t \sim [1, T], \mathbf{x}_0, \boldsymbol{\epsilon}_t} \|\boldsymbol{\epsilon}_t - \boldsymbol{\epsilon}_\theta(\mathbf{x}_t, t)\|_2^2. \quad (7)$$

Combined with Eq. (4), we can also obtain the predicted input image in one reverse step, i.e.,

$$\tilde{\mathbf{x}}_{0,t} = \frac{\mathbf{x}_t - \sqrt{1 - \bar{\alpha}_t}\boldsymbol{\epsilon}_\theta(\mathbf{x}_t, t)}{\sqrt{\bar{\alpha}_t}}. \quad (8)$$

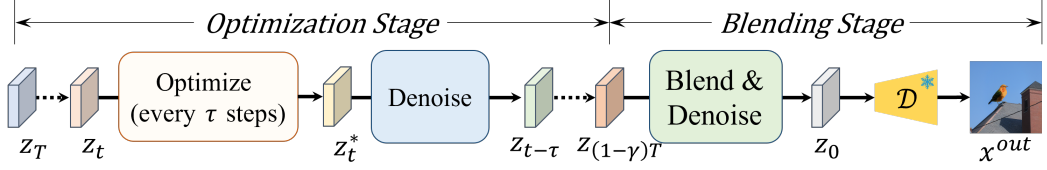
In the subsequent discussions, we denote $\tilde{\mathbf{x}}_{0,t}$ as the *one-step reconstruction*. As denoising progresses, $\tilde{\mathbf{x}}_{0,t}$ increasingly approximates the input data, ultimately reaching a denoising endpoint where it is identical to \mathbf{x}_0 .

4 Method

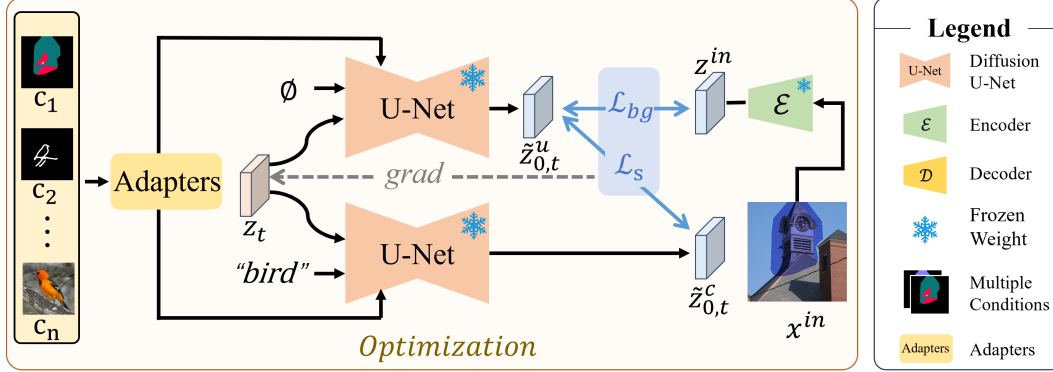
Our framework, summarized in Fig. 2, consists of two stages: the **optimization stage** and the **blending stage**. To better trade-off between image quality and computational efficiency, we introduce the coherence scale parameter γ . A larger γ leads to longer computation times but generates more coherent images.

4.1 Optimization Stage

Similar to image reconstruction [41, 42], we believe that the early stage of the reverse process determines the semantics of the generated image. Therefore, we interfere with the latent vectors using our optimization strategy to ensure the model comprehensively understands the entire image. Specifically, our optimization applies the gradients from the loss function we designed below during the reverse process in real time. In each optimization step, it seeks to find the optimal \mathbf{z}_t^* based on the one-step reconstructions $\tilde{\mathbf{z}}_{0,t}^u$ and $\tilde{\mathbf{z}}_{0,t}^c$. To alleviate the computational burden of the reverse diffusion, we sample the latent space and perform optimization every τ steps until $(1 - \gamma)T$.



(a) Full pipeline of PILOT.



(b) Illustration of our optimization strategy.

Figure 2: **Framework of our PILOT.** (a) First we apply our latent optimization strategy, where we adjust the direction of gradients and identify the optimal latent vector every τ steps, followed by the normal reverse diffusion process. After that, we apply the latent blending strategy until the denoising process is complete. (b) We depict how we optimize the latent vector with prompts from one or more modalities as conditions.

4.1.1 Loss function

Given an image x^{in} with a binary mask m , we obtain the latent representation z^{in} by feeding x^{in} into the pre-trained encoder \mathcal{E} , and get the resized mask m^d by downsample m to the shape of z^{in} . Under the framework of classifier-free guidance diffusion process [11], a two-branch structure is adopted. A shared text-to-image diffusion model outputs the prediction of the final latent variable $\tilde{z}_{0,t}^c$ with the text-guided embedding and $\tilde{z}_{0,t}^u$ with null-text embedding from z_t at step 0 from any timestep t , respectively. In the optimization iteration, each $\tilde{z}_{0,t}$ is obtained as

$$\tilde{z}_{0,t} = \tilde{z}_{0,t}^u + \omega(\tilde{z}_{0,t}^c - \tilde{z}_{0,t}^u), \quad (9)$$

where ω represents the text-guidance scale. It is important to note that gradients become ambiguous with respect to both terms when optimizing the entire $\tilde{z}_{0,t}$, which can result in unrealistic semantic overflow to the background region. To mitigate this shortage, we carefully design the losses based on each latent embedding $\tilde{z}_{0,t}^u$ and $\tilde{z}_{0,t}^c$.

Background Preservation Loss. As we depict the background region primarily with the information from null-text embedding from $\tilde{z}_{0,t}^u$, we first preserve the background via the loss

$$\mathcal{L}_{bg} = \left\| (\mathbb{1} - m^d) \odot \tilde{z}_{0,t}^u - (\mathbb{1} - m^d) \odot z^{in} \right\|_2^2, \quad (10)$$

where \odot represents the element-wise multiplication operation.

Semantic Centralization Loss. To depict the inpainted region close to the provided prompt, our objective is to maximize the disparity between $\tilde{x}_{0,t}^u$ and $\tilde{x}_{0,t}^c$ within the masked region. This implies centralizing the difference between $\tilde{z}_{0,t}^u$ and $\tilde{z}_{0,t}^c$ within the downsampled mask region. Hence, we

propose the *semantic centralization loss*

$$\begin{aligned}\mathcal{L}_s &= 1 - \frac{\|\mathbf{m}^d \odot \tilde{\mathbf{z}}_{0,t}^u - \mathbf{m}^d \odot \tilde{\mathbf{z}}_{0,t}^c\|_2^2}{\|\tilde{\mathbf{z}}_{0,t}^u - \tilde{\mathbf{z}}_{0,t}^c\|_2^2} \\ &= \frac{\|(\mathbf{1} - \mathbf{m}^d) \odot \tilde{\mathbf{z}}_{0,t}^u - (\mathbf{1} - \mathbf{m}^d) \odot \tilde{\mathbf{z}}_{0,t}^c\|_2^2}{\|\tilde{\mathbf{z}}_{0,t}^u - \tilde{\mathbf{z}}_{0,t}^c\|_2^2}.\end{aligned}\quad (11)$$

Constrained by the background loss, our objective is to minimize Eq. (11) to ensure that the difference between $\tilde{\mathbf{z}}_0^u$ and $\tilde{\mathbf{z}}_0^c$ in the background part is relatively small compared to the entire latent space.

Combining Eqs. (10) and (11) yields our overall loss function

$$\mathcal{L} = \mathcal{L}_{bg} + \lambda \mathcal{L}_s, \quad (12)$$

where λ is a coefficient that varies with the timestep. We run the optimization procedure to obtain optimal latent vectors $\tilde{\mathbf{z}}_{0,t}^{u*}$ and $\tilde{\mathbf{z}}_{0,t}^{c*}$ through minimizing Eq. (12) on time step t . Then, we obtain the final latent vector $\tilde{\mathbf{z}}_{0,t}^*$ via Eq. (9), and perform a denoising process. To better illustrate the process, an example is visualized in Appendix H.

4.1.2 Attention Mask

To prevent the overflow of semantic information and promote coherence, we design attention strategies in both cross-attention and self-attention. Although we can control most of the semantic information related to the condition to be generated within the mask region through our semantic centralization loss, there may still be some semantic information leaking into areas outside the mask region. To block semantic leaks to the background while keeping the inpainted regions consistent with the background, we incorporate the masked attention strategy.

Specifically, the attention matrix is modified by adding an attention mask \mathbf{M}^{attn} before the softmax layer, as

$$\mathcal{F} = \text{softmax}\left(\frac{\mathbf{Q}\mathbf{K}^T}{\sqrt{d}} + \mathbf{M}^{attn}\right)\mathbf{V}, \quad (13)$$

where $\mathbf{M}^{attn}(x, y)$ represents the relevance weight of \mathbf{K} to \mathbf{Q} , and d represents the dimension of \mathbf{Q} and \mathbf{K} .

First, we block the patch tokens in the background region from receiving any information from the prompt tokens. In the *cross-attention* layer, the query \mathbf{Q} is the image feature vector, and the key \mathbf{K} and the value \mathbf{V} are the text feature vectors. Hence, we use a mask to eliminate the influence of the text feature vector on the image feature vector outside the mask region. This yields

$$\mathbf{M}^{attn}(x, y) = \begin{cases} -\infty & \text{if } x \in S \\ 0 & \text{otherwise} \end{cases}, \quad (14)$$

where S represents the coordinates in the latent space corresponding to the unmasked part of the image.

Furthermore, the inpainted region has to be coherent with the background region and have no significant semantic differences. To this end, for the *self-attention* layer, where Q , K , and V are the image patch tokens, we use M^{attn} to eliminate the influence of the mask region on the revealed region of the image feature. The attention mask in self-attention is formulated as

$$\mathbf{M}^{attn}(x, y) = \begin{cases} -\infty & \text{if } x \in S \text{ and } y \notin S \\ 0 & \text{otherwise} \end{cases}. \quad (15)$$

However, applying this mask on the self-attention map during every pass through the U-Net in the optimization and denoising stages leads to inconsistencies between the masked region and other parts of the generated image. Therefore, in our experiments, while we employ the attention mask control approach on the cross-attention layer during both optimization and denoising, for the self-attention layer, we only apply it during the early stage of the denoising process. This strategy helps to better balance the consistency of image generation.

4.2 Blending Stage

After γT reverse steps, the core semantic information is already formed, and the diffusion process is primarily adding high-frequency details. The original diffusion process can effectively handle this. Therefore, to avoid extensive computation, we switch to using a latent blend operation [1] in the latter stage. Specifically, in each timestep, we blend the noisy version of the original background and the foreground region together as described in Eq. (16):

$$z_t = z_t^{bg} \odot (1 - m^d) + z_t^{fg} \odot m^d, \quad (16)$$

where z_t^{bg} is sampled by the forward process of diffusion model from the input latent embedding z^{in} , z_t^{fg} is the latent denoised from the previous timestep.

5 Experiments

5.1 Experimental setup

To ensure a fair comparison, we employ DDIM [27] as the diffusion sampler to generate results over 200 steps and set the classifier-free guidance scale ω to 7.5 following [11] for all methods used in our experiments. We set the coherence scale γ to 1, and optimize the latent variable every 10 steps along the denoising process, minimizing Eq. (12) by a 10-step SGD optimizer. The scheduler parameter λ is adaptively adjusted based on the size of the inpainting mask.

Datasets. For the text-guided inpainting task, we use the MS COCO [16] validation dataset, consisting of 5,000 images for evaluation. For each image, we randomly choose one object within the image and use its inflated segmentation map as the binary mask, defining the region to be inpainted.

Metrics. We primarily evaluate our model through two aspects: image generation quality and text-image alignment. For image quality assessment, we prefer Neural Image Assessment (NIMA) [28] over FID [9] due to its capability to measure quality based on human perception, which is more suitable for tasks like image editing or inpainting. More importantly, recent research [15] has highlighted FID’s limitations in text-to-image tasks, including its poor representation of diverse content, incorrect normality assumptions, and poor sample complexity.

Furthermore, we measure the text-image alignment between generated inpainting images and the text guidance by computing the average cosine similarity between their embeddings extracted by CLIP [22]. Additionally, we enlisted 30 human evaluators to assess the generated images, focusing on the visual quality of the generated images and the alignment between the images and the conditions. In this study, we employed 50 image sets for every assessment task, incorporating results from our PILOT and other baselines for comparative analysis. To minimize order bias, images in each set were presented side-by-side in a random sequence. Participants were tasked with ranking each image on a scale from 1 (worst) to 5 (best).

5.2 Comparisons of Text-guided and Spatial-controlled Inpainting

Text-guided Inpainting. We first compare our method with the state-of-the-art text-guided inpainting models that are **public available**: GLIDE [19], Blended Diffusion [2], Stable Diffusion Inpainting Model (SD-Inpaint) [24], and Uni-paint [37]. The text-guided editing results are shown in Fig. 3. Under various shapes and sizes of masks and different scenes, our model can generate images that are more realistic and better match the text than other methods, as shown in the last column of Fig. 3. Taking the third row as an example, the generated bike is intact and perfectly matches the text guidance "a blue bike parked on a sidewalk". Furthermore, the inpainting area and the background are consistent.

GLIDE [19] and Blended Diffusion [2] produce visually appealing images when text guidance is relatively simple and the mask is relatively small, as shown in the first row of Fig. 3. When the scenes in the images become complex and the known region of the image is minimal, they tend to generate images with poor visual effects, as shown in the second to fourth row of Fig. 3. Although SD-Inpaint [24] can generate visually acceptable pictures, it often encounters mismatches between the editing content and the text. Uni-paint [37] also suffers from inconsistencies where the contents between the mask region and the overall images appear discordant and abrupt.

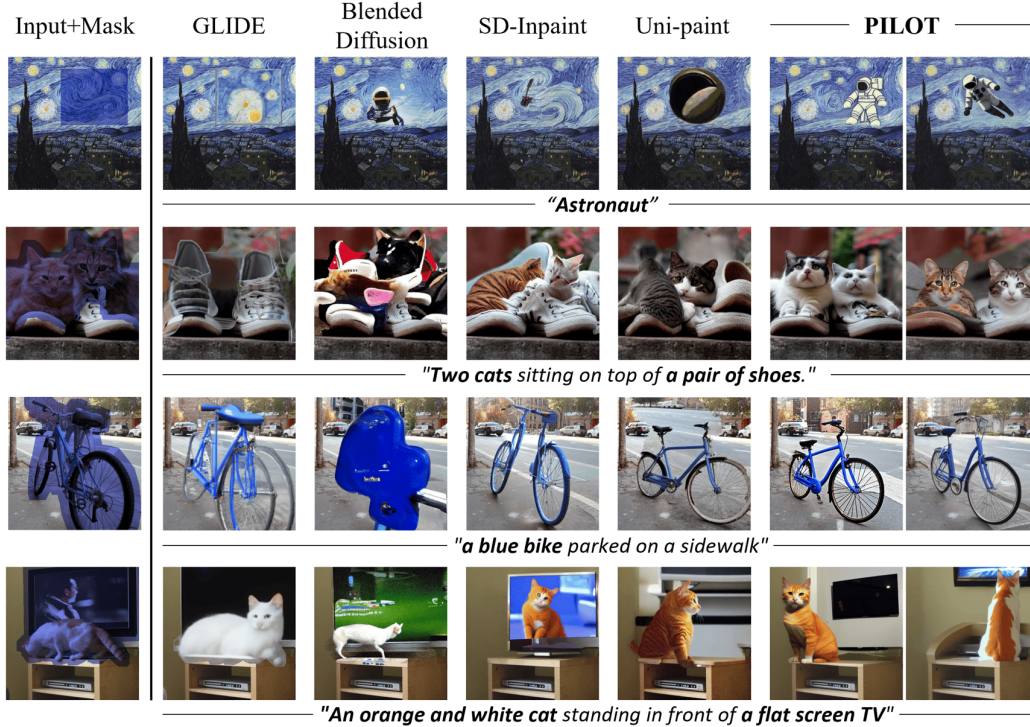


Figure 3: Qualitative comparison on text-guided image inpainting.

Table 1 presents the quantitative evaluation of our method and baselines on the text-guided image inpainting task. Blended Diffusion [2] and Uni-paint [37] have lower NIMA scores, indicating the poor visual quality of the images. We believe this is due to the inconsistencies introduced into the images by their blending operations. While SD-Inpaint [24] produces more high-quality images, it often fails to follow the text information to complete satisfactory inpainting. Compared with these SOTA methods, our method not only achieves the best quality of visual results with NIMA=5.443 but also aligns most closely with the text guidance according to CLIP-T=0.202, demonstrating the superiority of our optimization approach. For human evaluation, our method also gets the best scores for image quality and text matching, illustrating human preference for the images inpainted by our method rather than the SOTA ones.

Table 1: Quantitative evaluation of the text-guided image inpainting.

| Method | MS COCO | | Human Evaluation | |
|-----------------------|-----------------|-------------------|--------------------|--------------------------|
| | NIMA \uparrow | CLIP-T \uparrow | Quality \uparrow | Text Matching \uparrow |
| GLIDE [19] | 5.132 | 0.196 | 1.88 | 1.92 |
| Blended Diffusion [2] | 5.198 | 0.175 | 2.60 | 2.80 |
| SD-Inpaint [24] | 5.427 | 0.194 | 3.25 | 3.16 |
| Uni-paint [37] | 5.363 | 0.198 | 3.37 | 3.36 |
| PILOT | 5.453 | 0.202 | 3.84 | 3.71 |

Spatial-controlled Inpainting. We use ControlNet [40] to encode features from Canny maps, segmentation maps, sketches, etc., and add these encoded feature vectors to the original U-Net network to achieve spatial control of semantic information within the mask region. We compare our method with SD-Inpaint [24], Blended Latent Diffusion (BLD) [1], MaGIC [39]. Among them, SD-Inpaint and BLD, like our method, are based on Stable Diffusion v1-5 and use ControlNet to input spatial control information.

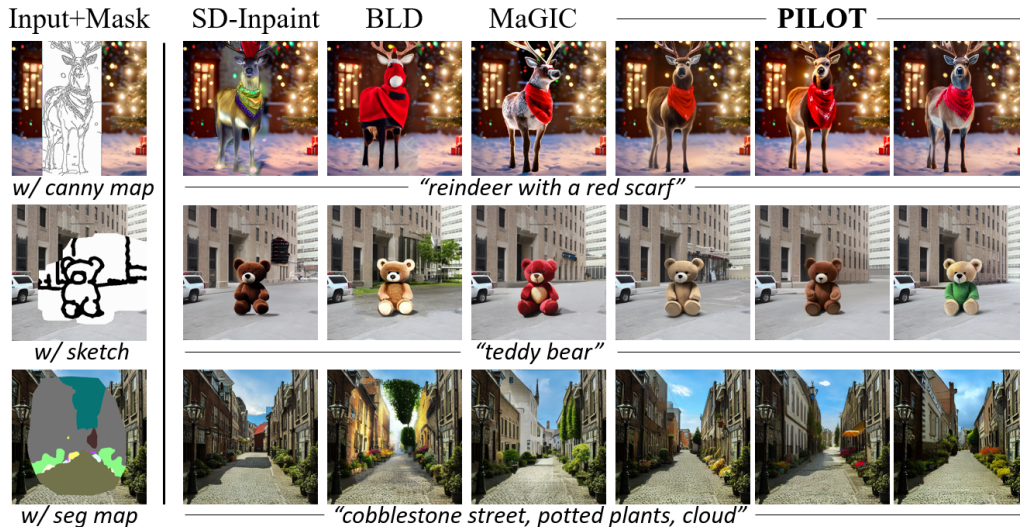


Figure 4: Qualitative comparison on text guided inpainting with spatial controls

As shown in Fig. 4, SD-Inpaint [24] does not integrate well with ControlNet [40], leading to inconsistencies between objects in the masked region and the background. For example, colors appearing behind a deer or the lighting on a bear do not blend well with the background. BLD produces incoherent results due to its poor understanding of the image content. MaGIC [39] generates relatively good visual effects, but there are still discrepancies between the generated subject’s spatial shape and the control information. For instance, the head and feet of the reindeer in the image do not correspond well to the canny map. Our method not only ensures coherence with spatial controls but also achieves a harmonious appearance.

For comparisons with subject-based inpainting and editing methods, please refer to Appendices D and E. Additionally, our method is compatible with other tools such as IP-Adapter [38] and T2I-Adapter [18], enabling the use of image prompts. See Appendix F for more details.

5.3 Ablation Study

Coherence Scale. We illustrate the impact of the coherence scale on the generated results and computation time t in Fig. 5. In this example, we adopt a 30-step denoising process and perform gradient descent optimization five times every three denoising steps during the optimization stage, tested on an NVIDIA GeForce RTX 3090 GPU.

We observe that as γ increases, the coherence of the image improves due to more optimization steps involved. However, the computation time t also increases. When γ is 0, it is equivalent to the blended latent diffusion process with an attention mask, but without any optimization of the latent space. This results in a significant color difference between the masked region and the surrounding environment. We can generate high-quality images with reasonable time consumption. Therefore, in practice, we recommend choosing $\gamma = 0.5$.

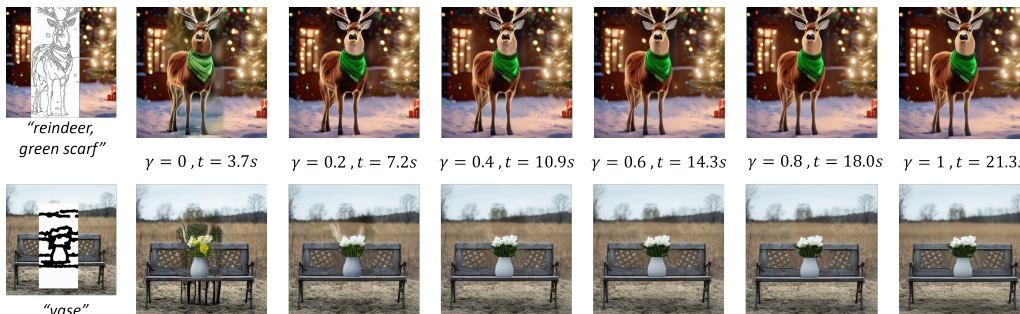


Figure 5: Ablation study on the coherence scale γ .

6 Conclusion

We have introduced PILOT, a framework that intervenes in the latent vector of the diffusion reverse process using gradients based on our proposed loss function dynamically. Developed on top of classifier-free guidance diffusion, our method seamlessly integrates into any pre-trained networks, accommodating multiple modalities as conditions to achieve coherent inpainted images. Experiments across various inpainting settings have demonstrated the superiority of our method in terms of generation quality, as well as its ability to closely match the prompt inputs. These results are validated by quantitative metrics and human evaluation.

Limitation. While Imagen Editor [32] and SmartBrush [34] demonstrate strong performance in text-guided inpainting, a direct comparison with our PILOT model is currently not possible due to the unavailability of their code. Additionally, our current version of PILOT utilizes Stable Diffusion v1-5 [24]. Since Stable Diffusion XL [21] offers superior generation capabilities, we plan to integrate PILOT to this version in the future.

References

- [1] Omri Avrahami, Ohad Fried, and Dani Lischinski. Blended latent diffusion. *ACM Transactions on Graphics (TOG)*, 42(4):1–11, 2023. 1, 2, 3, 7, 8
- [2] Omri Avrahami, Dani Lischinski, and Ohad Fried. Blended diffusion for text-driven editing of natural images. In *Proceedings of the IEEE/CVF Conference on Computer Vision and Pattern Recognition*, pages 18208–18218, 2022. 2, 3, 7, 8
- [3] Manuel Brack, Felix Friedrich, Dominik Hintersdorf, Lukas Struppek, Patrick Schramowski, and Kristian Kersting. Sega: Instructing diffusion using semantic dimensions. *arXiv preprint arXiv:2301.12247*, 2023. 3
- [4] Manuel Brack, Felix Friedrich, Katharina Kornmeier, Linoy Tsaban, Patrick Schramowski, Kristian Kersting, and Apolinário Passos. Ledits++: Limitless image editing using text-to-image models. *arXiv preprint arXiv:2311.16711*, 2023. 13, 16
- [5] Tim Brooks, Aleksander Holynski, and Alexei A Efros. Instructpix2pix: Learning to follow image editing instructions. In *Proceedings of the IEEE/CVF Conference on Computer Vision and Pattern Recognition*, pages 18392–18402, 2023. 1, 3, 13, 16
- [6] Xi Chen, Lianghua Huang, Yu Liu, Yujun Shen, Deli Zhao, and Hengshuang Zhao. Anydoor: Zero-shot object-level image customization. *arXiv preprint arXiv:2307.09481*, 2023. 13, 15
- [7] Guillaume Couairon, Jakob Verbeek, Holger Schwenk, and Matthieu Cord. Diffedit: Diffusion-based semantic image editing with mask guidance. *arXiv preprint arXiv:2210.11427*, 2022. 13, 16
- [8] Amir Hertz, Ron Mokady, Jay Tenenbaum, Kfir Aberman, Yael Pritch, and Daniel Cohen-Or. Prompt-to-prompt image editing with cross attention control. *arXiv preprint arXiv:2208.01626*, 2022. 3
- [9] Martin Heusel, Hubert Ramsauer, Thomas Unterthiner, Bernhard Nessler, and Sepp Hochreiter. Gans trained by a two time-scale update rule converge to a local nash equilibrium. *Advances in neural information processing systems*, 30, 2017. 7
- [10] Jonathan Ho, Ajay Jain, and Pieter Abbeel. Denoising diffusion probabilistic models. *Advances in neural information processing systems*, 33:6840–6851, 2020. 3, 4
- [11] Jonathan Ho and Tim Salimans. Classifier-free diffusion guidance. *arXiv preprint arXiv:2207.12598*, 2022. 5, 7
- [12] Edward J Hu, Yelong Shen, Phillip Wallis, Zeyuan Allen-Zhu, Yuanzhi Li, Shean Wang, Lu Wang, and Weizhu Chen. Lora: Low-rank adaptation of large language models. *arXiv preprint arXiv:2106.09685*, 2021. 2

- [13] Wenjing Huang, Shikui Tu, and Lei Xu. Pfb-diff: Progressive feature blending diffusion for text-driven image editing. *arXiv preprint arXiv:2306.16894*, 2023. 3
- [14] Inbar Huberman-Spiegelglas, Vladimir Kulikov, and Tomer Michaeli. An edit friendly ddpn noise space: Inversion and manipulations. *arXiv preprint arXiv:2304.06140*, 2023. 3
- [15] Sadeep Jayasumana, Srikumar Ramalingam, Andreas Veit, Daniel Glasner, Ayan Chakrabarti, and Sanjiv Kumar. Rethinking fid: Towards a better evaluation metric for image generation. *arXiv preprint arXiv:2401.09603*, 2023. 7
- [16] Tsung-Yi Lin, Michael Maire, Serge Belongie, James Hays, Pietro Perona, Deva Ramanan, Piotr Dollár, and C Lawrence Zitnick. Microsoft coco: Common objects in context. In *Computer Vision—ECCV 2014: 13th European Conference, Zurich, Switzerland, September 6-12, 2014, Proceedings, Part V 13*, pages 740–755. Springer, 2014. 7
- [17] Ron Mokady, Amir Hertz, Kfir Aberman, Yael Pritch, and Daniel Cohen-Or. Null-text inversion for editing real images using guided diffusion models. In *Proceedings of the IEEE/CVF Conference on Computer Vision and Pattern Recognition*, pages 6038–6047, 2023. 3
- [18] Chong Mou, Xintao Wang, Liangbin Xie, Yanze Wu, Jian Zhang, Zhongang Qi, and Ying Shan. T2i-adapter: Learning adapters to dig out more controllable ability for text-to-image diffusion models. In *Proceedings of the AAAI Conference on Artificial Intelligence*, volume 38, pages 4296–4304, 2024. 3, 9, 13, 17
- [19] Alex Nichol, Prafulla Dhariwal, Aditya Ramesh, Pranav Shyam, Pamela Mishkin, Bob McGrew, Ilya Sutskever, and Mark Chen. Glide: Towards photorealistic image generation and editing with text-guided diffusion models. *arXiv preprint arXiv:2112.10741*, 2021. 3, 7, 8
- [20] Gaurav Parmar, Krishna Kumar Singh, Richard Zhang, Yijun Li, Jingwan Lu, and Jun-Yan Zhu. Zero-shot image-to-image translation. In *ACM SIGGRAPH 2023 Conference Proceedings*, pages 1–11, 2023. 3
- [21] Dustin Podell, Zion English, Kyle Lacey, Andreas Blattmann, Tim Dockhorn, Jonas Müller, Joe Penna, and Robin Rombach. Sdxl: Improving latent diffusion models for high-resolution image synthesis. *arXiv preprint arXiv:2307.01952*, 2023. 10
- [22] Alec Radford, Jong Wook Kim, Chris Hallacy, Aditya Ramesh, Gabriel Goh, Sandhini Agarwal, Girish Sastry, Amanda Askell, Pamela Mishkin, Jack Clark, et al. Learning transferable visual models from natural language supervision. In *International conference on machine learning*, pages 8748–8763. PMLR, 2021. 7
- [23] Aditya Ramesh, Prafulla Dhariwal, Alex Nichol, Casey Chu, and Mark Chen. Hierarchical text-conditional image generation with clip latents, 2022. URL <https://arxiv.org/abs/2204.06125>, 7, 2022. 1
- [24] Robin Rombach, Andreas Blattmann, Dominik Lorenz, Patrick Esser, and Björn Ommer. High-resolution image synthesis with latent diffusion models. In *Proceedings of the IEEE/CVF conference on computer vision and pattern recognition*, pages 10684–10695, 2022. 1, 7, 8, 9, 10
- [25] Nataniel Ruiz, Yuanzhen Li, Varun Jampani, Yael Pritch, Michael Rubinstein, and Kfir Aberman. Dreambooth: Fine tuning text-to-image diffusion models for subject-driven generation. In *Proceedings of the IEEE/CVF Conference on Computer Vision and Pattern Recognition*, pages 22500–22510, 2023. 2, 15
- [26] Chitwan Saharia, William Chan, Huiwen Chang, Chris Lee, Jonathan Ho, Tim Salimans, David Fleet, and Mohammad Norouzi. Palette: Image-to-image diffusion models. In *ACM SIGGRAPH 2022 Conference Proceedings*, pages 1–10, 2022. 3
- [27] Jiaming Song, Chenlin Meng, and Stefano Ermon. Denoising diffusion implicit models. *arXiv preprint arXiv:2010.02502*, 2020. 7
- [28] Hossein Talebi and Peyman Milanfar. Nima: Neural image assessment. *IEEE transactions on image processing*, 27(8):3998–4011, 2018. 7

- [29] Linoy Tsaban and Apolinário Passos. Ledits: Real image editing with ddpm inversion and semantic guidance. *arXiv preprint arXiv:2307.00522*, 2023. 3
- [30] Bram Wallace, Akash Gokul, and Nikhil Naik. Edict: Exact diffusion inversion via coupled transformations. In *Proceedings of the IEEE/CVF Conference on Computer Vision and Pattern Recognition*, pages 22532–22541, 2023. 3
- [31] Qixun Wang, Xu Bai, Haofan Wang, Zekui Qin, and Anthony Chen. Instantid: Zero-shot identity-preserving generation in seconds. *arXiv preprint arXiv:2401.07519*, 2024. 3
- [32] Su Wang, Chitwan Saharia, Ceslee Montgomery, Jordi Pont-Tuset, Shai Noy, Stefano Pellegrini, Yasumasa Onoe, Sarah Laszlo, David J Fleet, Radu Soricut, et al. Imagen editor and editbench: Advancing and evaluating text-guided image inpainting. In *Proceedings of the IEEE/CVF Conference on Computer Vision and Pattern Recognition*, pages 18359–18369, 2023. 1, 3, 10
- [33] Chen Henry Wu and Fernando De la Torre. Unifying diffusion models’ latent space, with applications to cyclediffusion and guidance. *arXiv preprint arXiv:2210.05559*, 2022. 3
- [34] Shaoan Xie, Zhifei Zhang, Zhe Lin, Tobias Hinz, and Kun Zhang. Smartbrush: Text and shape guided object inpainting with diffusion model. In *Proceedings of the IEEE/CVF Conference on Computer Vision and Pattern Recognition*, pages 22428–22437, 2023. 1, 10
- [35] Sihan Xu, Yidong Huang, Jiayi Pan, Ziqiao Ma, and Joyce Chai. Inversion-free image editing with natural language. *arXiv preprint arXiv:2312.04965*, 2023. 13, 16
- [36] Binxin Yang, Shuyang Gu, Bo Zhang, Ting Zhang, Xuejin Chen, Xiaoyan Sun, Dong Chen, and Fang Wen. Paint by example: Exemplar-based image editing with diffusion models. In *Proceedings of the IEEE/CVF Conference on Computer Vision and Pattern Recognition*, pages 18381–18391, 2023. 13, 15
- [37] Shiyuan Yang, Xiaodong Chen, and Jing Liao. Uni-paint: A unified framework for multimodal image inpainting with pretrained diffusion model. In *Proceedings of the 31st ACM International Conference on Multimedia*, pages 3190–3199, 2023. 3, 7, 8, 13, 15
- [38] Hu Ye, Jun Zhang, Sibao Liu, Xiao Han, and Wei Yang. Ip-adapter: Text compatible image prompt adapter for text-to-image diffusion models. *arXiv preprint arXiv:2308.06721*, 2023. 1, 3, 9, 13, 17
- [39] Yongsheng Yu, Hao Wang, Tiejian Luo, Heng Fan, and Libo Zhang. Magic: Multi-modality guided image completion. *arXiv preprint arXiv:2305.11818*, 2023. 1, 8, 9
- [40] Lvmin Zhang, Anyi Rao, and Maneesh Agrawala. Adding conditional control to text-to-image diffusion models. In *Proceedings of the IEEE/CVF International Conference on Computer Vision*, pages 3836–3847, 2023. 1, 3, 8, 9, 13
- [41] Tong Zhang and Fatih Porikli. Sparse coding on cascaded residuals. In *Computer Vision—ACCV 2016: 13th Asian Conference on Computer Vision, Taipei, Taiwan, November 20–24, 2016, Revised Selected Papers, Part IV 13*, pages 19–34. Springer, 2017. 2, 4
- [42] Tong Zhang and Fatih Porikli. Cascade residuals guided nonlinear dictionary learning. *Computer Vision and Image Understanding*, 173:86–97, 2018. 2, 4
- [43] Shihao Zhao, Dongdong Chen, Yen-Chun Chen, Jianmin Bao, Shaozhe Hao, Lu Yuan, and Kwan-Yee K Wong. Uni-controlnet: All-in-one control to text-to-image diffusion models. *Advances in Neural Information Processing Systems*, 36, 2024. 3

Supplementary Material

Contents of the appendix

The contents of the supplementary material are organized as follows:

- In Appendix **A**, we explain the implementation details of PILOT, including the scheduler of λ and the learning rate.
- In Appendix **B**, we discuss the impact of the mask attention strategy.
- In Appendix **C**, we discuss the impact of the optimization interval τ .
- In Appendix **D**, we compare our method with existing subject-based inpainting methods such as Paint-by-Example [36], Uni-paint [37] and Anydoor [6].
- In Appendix **E**, we compare our method with existing image editing methods such as Instruct-Pix2Pix [5], LEDITS++ [4], DiffEdit [7] and InfEdit [35].
- In Appendix **F**, we show more multi-modality inpainting results by combining PILOT with adapters such as ControlNet [40], IP-Adapter [38], and T2I-Adapter [18].
- In Appendix **G**, we show how we achieve fine-grain editing with multi-modality controls and personalized text-to-image models.
- In Appendix **H**, we visualize the process of the inpainting process.
- In Appendix **I**, we show more results of text-guided image inpainting.
- In Appendix **J**, we show the details of our user study on text-guided inpainting.
- In Appendix **K**, we discuss the societal impact of our method.

A Implementation Details

The scheduler parameter λ is adaptively adjusted based on the size of the inpainting mask. We found that setting λ to be proportional to the square of the unmasked region’s area yields optimal results. Specifically, when the unmasked area constitutes one-third of the total image area, setting λ to 110 produces excellent outcomes.

The learning rate for optimization follows an exponential decay with respect to the denoising timestep. When using only the stable diffusion model for inpainting, we set the learning rate at timestep $0.95T$ to 0.03. However, when inpainting with the ControlNet-extended stable diffusion model, we increase the learning rate at timestep $0.95T$ to 0.05. This adjustment is because the additional spatial features provided by ControlNet make it easier for the model to find the accurate gradient direction, ensuring that the background of the one-step reconstruction matches the background of the input. This enables the use of a larger learning rate to facilitate faster convergence.

For practical use, we employ multi-modality inpainting with ControlNet, utilizing 30 denoising steps. We perform optimization every 3 steps using 3 steps of gradient descent, and set the coherence scale to 0.4, resulting in a total of 15 optimization steps. This approach yields satisfactory results and takes approximately 8 seconds on an NVIDIA GeForce RTX 3090 GPU.

B Discussion of the mask attention strategy

In Fig. 6, we demonstrate the impact of the attention mask on image inpainting. Without an attention mask, the denoising network may inaccurately perceive parts of the object as outside the mask region, leading to a misinterpretation of the image’s structure. Introducing a cross-attention mask helps mitigate these issues, resulting in generated content in the mask region that closely aligns with the provided prompt. However, inconsistencies may still arise between the mask region and the rest of the image, particularly at the boundary, leading to unnatural appearances. Although blocking self-attention among the image tokens can alleviate these inconsistencies, it may also result in abrupt color changes at the edges, compromising overall image coherence. In our approach, we use the self-attention mask only during the early denoising stages to ensure object integrity while maintaining scene coherence.



Figure 6: Ablation study on attention mask control. Best viewed with zoom-in.

C Discussion of the optimization interval

To explore how the optimization interval τ influences the outcomes of edits, we set $\gamma = 1$ and vary the optimization interval while maintaining a total of 200 steps for both denoising and optimization processes. As shown in Fig. 7, the outcomes with a moderate value of τ are better than other ones.

We observe that the visual quality of the main subject is poor at small intervals, such as 1 and 3. Small intervals indicate the excessive frequency of optimization, which slightly deviates the generation trajectory from the model’s output domain. When the interval is large, $\tau = 40$ as an example, significant inconsistency arises. It is due to the large interval causes a delay in aligning the mask region with the background details.

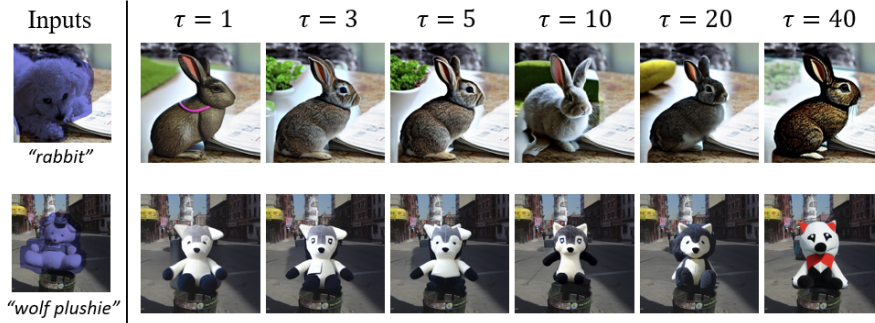


Figure 7: Ablation study of the optimization interval.

D Comparisons with Subjected-based Inpainting Methods

To assess the effectiveness of our personalized editing, we utilize personalized text-to-image models based on given subjects trained with DreamBooth [25] to achieve subject-driven inpainting and compare our method with Paint-by-Example (PBE) [36], Uni-paint [37] and AnyDoor [6]. Note that, PBE [36], Uni-paint [37], and AnyDoor [6] employ a reference subject image to direct the generative process, while our method employs a subject-driven pre-trained model, whose output domain includes information about the subject, enabling the precise inpainting of the subject into the image’s missing mask.

As shown in Fig. 8, our method retains more details of the corresponding objects and produces images that look more like real photos. Although PBE [36] and Uni-paint [37] generate subject-driven inpainting images that appear natural, they fail when the reference object has a lot of details. It misunderstands the object’s structure, which leads to the inpainting images suffering significant differences from the reference object in color and texture, such as the bear plushie shown in Fig. 8. AnyDoor [6] draws objects closer to the reference in terms of color and shape, but the generated subjects often appear incongruous with the background, as seen with the vase in the last row of Fig. 8. More customized inpainting results are shown in Fig. 9, which demonstrates the subject can be applied to various scenarios with coherence and good quality.



Figure 8: Qualitative comparison on subject-driven inpainting with SOTA methods.



Figure 9: Personalized image editing examples with the guidance of subject.

E Comparisons with Image Editing Methods

We compared our method with Instruct-Pix2Pix [5], LEDITS++ [4], DiffEdit [7] and InfEdit [35], which are state-of-the-art image editing techniques, as illustrated in Fig. 10.

We can observe that these editing methods often fail to accurately locate the region corresponding to the descriptive words, resulting in the semantic description being applied to the wrong area. Even when they successfully edit the described region, other areas outside the target region are also affected. In contrast, our method uses a masked image and text as conditions, allowing edits to be confined to the specified region. Additionally, we can incorporate the shape information of objects from the original image as spatial guidance, ensuring that the shape of the objects remains largely unchanged during editing.

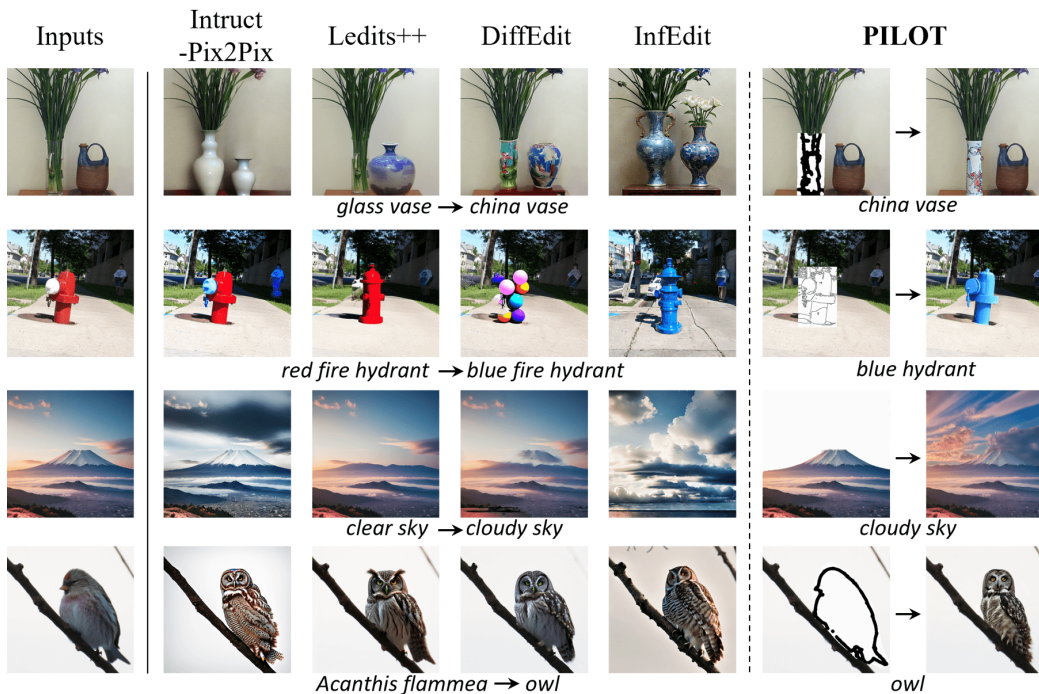


Figure 10: Comparison with editing methods.

F Compatible with Various Adapters

We show more spatial-controlled inpainting results achieved by combining PILOT with ControlNet in Fig. 11. Our method is also compatible with other adapters such as IP-Adapter [38] and T2I-Adapter [18], enabling image prompt and spatial controls, as illustrated in Fig. 12.

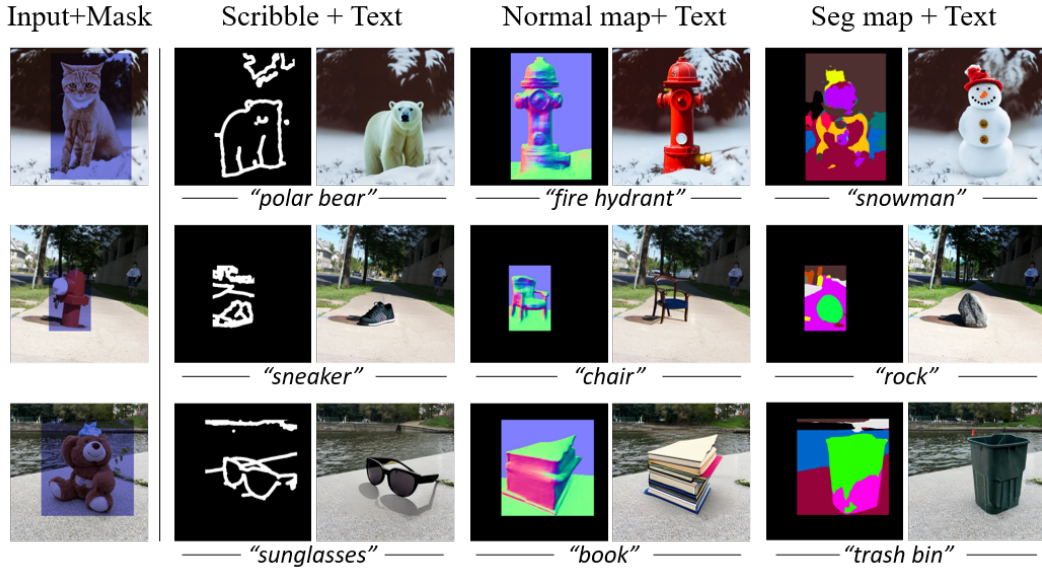


Figure 11: Qualitative comparison of multi-modality-based image inpainting (scribble, normal map, and segmentation map with text).

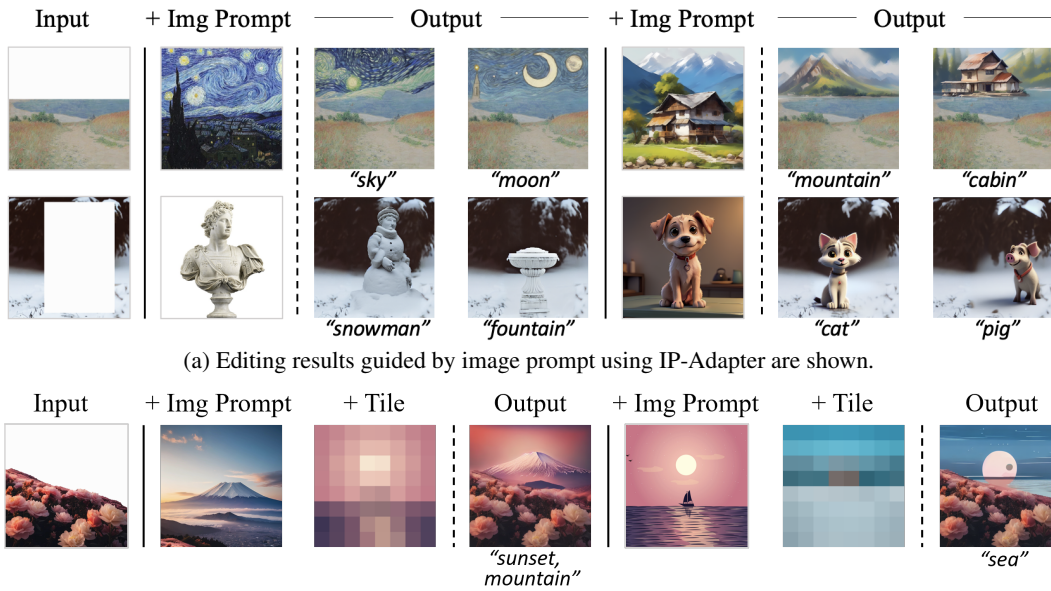


Figure 12: Combining PILOT with IP-Adapter and T2I-adapter, we achieve image inpainting guided by image prompts and spatial controls.

G Fine-grained Editing

In personalized pre-trained text-to-image diffusion models, users often struggle to edit local regions with precise control without compromising the consistency of the generated images. Our fine-tuning-free method offers the opportunity to conduct a series of accurate local part generations, aligning with the users’ designs. We utilize a Disney-style pretrained Stable Diffusion² and Monet-style LORA³ as the generator respectively, employing both text and scribbles to edit the image step by step, shown in Fig. 13. In each edit, our method keeps the unmasked region well while generating the desired region based on users’ interactions.

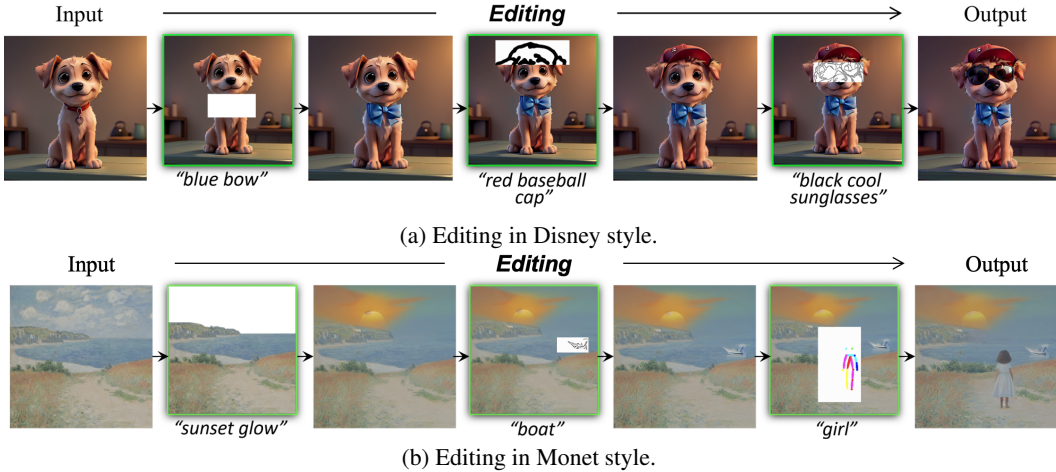


Figure 13: Generating fine-grained parts according to user interaction through multiple steps. White boxes denote the masked region, with three different text prompts serving as conditions. Additionally, in the second and third edits, we incorporate scribbles to achieve more accurate control.

H Visualization of Denoising Process

As depicted in Fig. 14, during the initial phase of the denoising process, our method primarily focuses on aligning the semantics. As the semantic alignment stabilizes, the denoising process transitions to enhance the overall image quality. Additionally, as the one-step reconstruction approaches the background, the gradients from our optimization diminish, resulting in fewer changes.

I Additional results

Given a specific source image, mask, and conditions, our model is capable of generating coherent yet diverse results, as illustrated in Fig. 15.

²downloaded from <https://huggingface.co/stablediffusionapi/disney-pixar-cartoon>

³downloaded from <https://civitai.com/models/73902/claude-monetoscar-claude-monet-style>

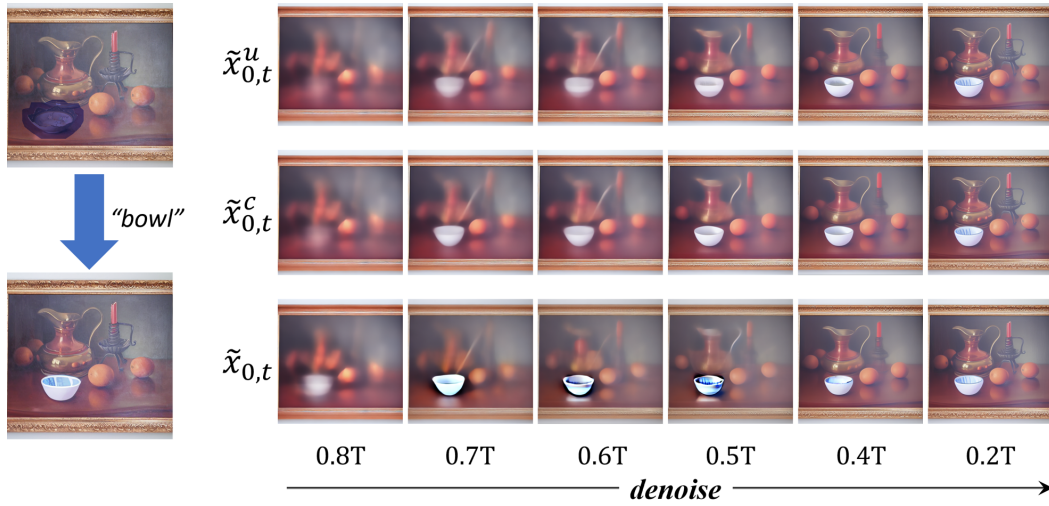


Figure 14: Images generated by using one-step reconstruction of latent vector $\tilde{z}_{0,t}^{u*}$, $\tilde{z}_{0,t}^{c*}$, and $\tilde{z}_{0,t}^*$ at different diffusion steps.



Figure 15: The reconstruction results of our PILOT with the same single-modality prompts but different random seeds.

J User study

We conducted our surveys on Amazon Mechanical Turk (MTurk), where each participant was tasked with ranking the image results produced by our method and the baseline methods based on a given question. To ensure fairness, the results from different methods were presented in a random order, and participants were not informed about which method each image belonged to before submitting their answers. The survey interfaces are depicted in Fig. 16.

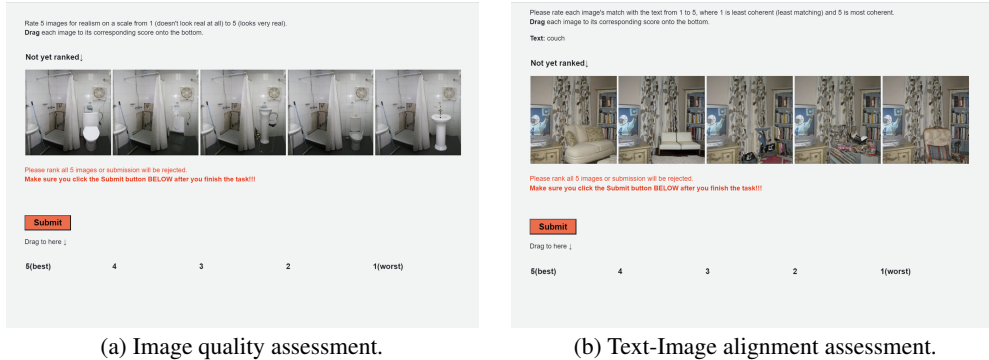


Figure 16: Survey interfaces for human evaluation of text-guided image inpainting results.

K Societal Impact

The remarkable capability of PILOT to effectively edit images raises concerns about its potential misuse for generating deceptive or misleading images, such as synthetic media and deepfakes. While the advancements in image inpainting can benefit numerous fields, including art restoration, film production, and personalized content creation, they also pose ethical and societal risks. The ease of altering images can lead to the spread of misinformation, compromising the integrity of visual media.

To address these concerns, we will make the source code of our method publicly available. This transparency will enable the research community and broader society to scrutinize its implementation, ensuring that its development and application adhere to ethical standards. Furthermore, we encourage the implementation of robust watermarking and authentication technologies to detect and mitigate the creation and distribution of manipulated media. By fostering an open dialogue about the ethical use of image inpainting technology, we aim to balance innovation with responsibility, ensuring that the benefits of our research are realized while minimizing potential harm.